Proceedings of 20th International Congress on Acoustics, ICA 2010

23-27 August 2010, Sydney, Australia

On the influence of transducer heating in underwater ultrasonic thrusters

Alfred C. H. Tan (1), and Franz S Hover (1)

(1) Department of Mechanical Engineering, Massachusetts Institute of Technology, 77 Massachusetts Ave, Cambridge, MA 02139 USA

PACS: 43.25.Nm, 43.35.Ty, 43.35.Ud, 43.35.Yb

ABSTRACT

An ultrasonic thruster (UST) is defined as a piezoelectric actuator excited at ultrasonic frequencies, generating high-power acoustic waves so as to produce bulk fluid movement for propulsion underwater. The thrust force is associated with the decrease in mean momentum flux which results from acoustic energy loss in the medium, and can be intensified through finite-amplitude ultrasound. These transducers do not convert all their electrical power into acoustical energy; rather, significant heat is dissipated through the transducer surface. Indeed, heating from intense ultrasound – on the order of 100Wcm^{-2} – is observable to the naked eye as the water next to the transducer heats up. In our past studies, we found that the UST has an inherently low acoustic efficiency, especially with high electrical power levels. In this study, we quantify experimentally the amount of heat loss through the transducer surface, and introduce a dimensionless parameter to relate this loss with the electrical power supplied to the transducer, which also corresponds with thrust and acoustic power. Heat energy dissipated through the transducer surface correlates with a decrease in the thrust production. Understanding of this phenomenon should help engineers to design a transducer system that can minimize heat losses and improve thrust production.

INTRODUCTION

At very small scales, propulsors such as traditional rotary propellers or impellers will impose significant complexity, fabrication, reliability issues. Further, at very low Reynolds numbers, small-scale propulsors may experience disproportionate viscous losses, with a high sensitivity to surface roughness [1]. Such intricate devices are more susceptible to biofouling and corrosion. In addition, cheap COTS components for such devices are not available today [2].

In this paper we explore a newer propulsion technology using ultrasound; the device uses a piezoelectric transducer (PZT) to transmit high power, high frequency ultrasound into the fluid medium [3]. We call it ultrasonic thruster (UST). The propulsive mechanism can be briefly described as a loss in momentum flux along the acoustic transmission path due to absorption, leading to a net force which is associated with the thrust acting on the transducer. Thrust generated is in the order of several milli-newtons for a transducer size of 1cm. The device is robust because it has no moving parts beyond the membrane, and can be flush-mounted to a watercraft. The UST we describe below can achieve an average sound intensity of 132dB (re 1μPa) and is destructive to biofouling [4].

As we have observed in our previous work [3], acoustic efficiency deteriorates as the power applied to the UST is increased (> 70W). As in all PZTs, electrical energy is converted into heat and acoustic power. In the presence of a large electric field, heat dissipation increases significantly, depending on the dielectric dissipation factor, capacitance, and the presence of heat retardant materials next to the PZT. In instances of high power, localized heating at the soldered points may result in a failure or other undesirable outcome [5].

While temperature studies on PZT have been adequately described and investigated in the literature [6-8], we are not aware of any work that makes a direct connection between temperature rise and propulsive thrust generated. We made thermal measurements on the surface of the transducer under ultrasonic thrusting conditions, and gain a fuller understanding of the UST design issues. As the UST is an underwater propulsor, knowledge of the conditions leading it to become a thermal source would aid in the transducer and system design. The following sections lay out the theoretical background for heat transfer through the transducer, and its acoustic efficiency, and show the experimental results indicating what are the critical design points.

HEAT TRANSFER AND ULTRASONIC THRUST

Heat transfer

Figure 1 shows the sectional view of the UST. Two o-rings are designed to seal the PZT against the water pressure and the air-backed layer provides maximum power transfer into the water. The screwed-on base holding the transducer is made from Telfon, and the capping component holding the o-rings too. The adhesive heat shrink and silicone potting seal the water from entering the air backing.

The transducer material and medium will determine the heat transfer profile, rate of heat transfer and its dominant mode of heat transfer. For effective propulsion purpose, we add a

layer of epoxy cast to match the acoustic impedance between the PZT and water.

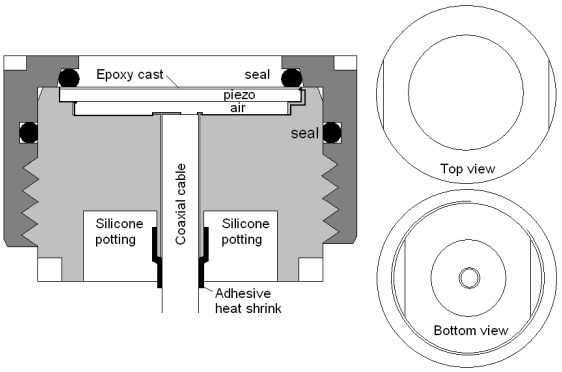

Figure 1. Construction of the modular UST. A female Teflon cap is screwed onto the base holder which holds the transducer. O-rings provide the water-tight seals, and silicone potting provides flexibility and waterproofing where the coaxial cable exits.

From Figure 2, in order to calculate the temperature profile through the transducer, $x = 0$ is taken at the centreline through the thickness of the transducer and the average temperature at the centerline is given by

$$T_{mid} = \frac{Q_p x_p}{2k_p A_p}\left(\frac{1}{\pi^2}+\frac{1}{4}\right)+T_p \qquad (1)$$

where x_p (m) is the thickness of the transducer, k_p (W/m·°C) is the thermal conductivity of the transducer, A_p (m^2) is the surface area of the transducer, and T_p (°C) is the temperature at the interface between the transducer and epoxy layer [8]. Q_p (W) is the average heat transfer rate of the piezoelectric material, which is also the average power dissipation, given by

$$Q_p = 2\pi f C \tan\delta E_{rms}^2 \qquad (2)$$

where f (Hz) is the resonance frequency, C (F) is the capacitance of the transducer, tan δ (%) is the dielectric dissipation factor, and E_{rms} (V) is the root-mean-square of the applied voltage. It is important to understand that under high power and temperature conditions, the transducer's dielectric dissipation factor will change with the voltage applied, temperature and fluidic load. Consequently, the capacitance and dielectricity also vary nonlinearly as the voltage and temperature increase, incurring significant errors if these are not carefully characterized under elevated settings. The temperature profile of the piezoelectric material takes on a parabolic distribution, peaking at T_{mid} (°C), and either surface of the transducer has the same temperature, T_p.

The 1-dimensional Fourier's law used to describe the thermal conduction of heat through the layer of epoxy cast on the UST surface, and is governed by the heat flux, q (W/m^2), and the heat transfer rate (W) is given by

$$Q_e = qA_e = k_e A_e \frac{\left(T_p - T_e\right)}{x_e} \qquad (3)$$

where k_e (W/m·°C) is the thermal conductivity, T_e (°C) is the surface temperature of the epoxy cast facing the water, and x_e (m) is the thickness of the epoxy cast. q will be positive if heat flows along the x-direction, and vice versa.

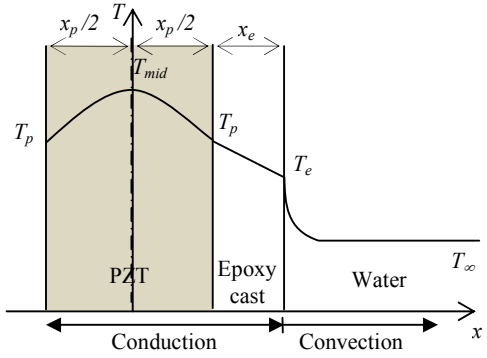

Figure 2. A schematic diagram of the heat transfer profile. Acoustic transmission is generated by a transducer made from a PZT, through an epoxy cast layer into the water. Temperature gradient in each material outlines their relative heat transmission.

As heat transfers into the water, convection will be dominant (heat radiation is negligible in our case) and using the steady-state Newton's Law of cooling, the convection governing equation is describe as

$$Q_c = \bar{h} A_c \left(T_e - T_\infty\right) \qquad (4)$$

where $\bar{h}$ is the averaged convective heat transfer (W/m^2·°C), A_c is the area of transducer exposed to the water (m^2), and T_∞ is the ambient water tank temperature (°C).

Acoustic power and ultrasonic thrust

The detailed mathematical treatment for the electrical power applied on the transducer, acoustic power and the output thrust generated can be found in the references [9, 10]. We will only outline the connection between acoustic power, P (W), and the thrust generated, *Thrust* (N), by a reduced formula, and introducing an acoustic efficiency factor, η, to account for the electromechanical coupling losses into the water in converting the ultrasonic energy, by

$$P_x = \frac{c \times Thrust}{\eta} \qquad (5)$$

where $P_x = \rho c \upsilon_o^2 a^2 \pi \int_0^{\theta_1} \frac{J_1(ka\sin\theta)}{\sin\theta} d\theta$ (W) is the acoustic power transmitted through the surface of the UST along the axial, and ρ (kg/m^3) is the density, c (m/s) is the speed of sound, υ_o (m/s) is the surface velocity of the transducer, a (m) is the radius of the transducer, k is the wave number, θ is the elevation angle from the axial, and $J_1(\cdot)$ is the Bessel function of the first kind. Thrust can also be shown as $Thrust = \rho \upsilon_o^2 a^2 \pi \int_0^{\theta_1} \frac{J_1(ka\sin\theta)}{\sin\theta} d\theta$ (W), where the parameters were already denoted in the above. Note that at the surface of the transducer, the electrical power applied to the transducer, P, is described by the square of root-mean-square of input voltage, E_{rms}, divided by the real component of the transducer impedance, $\Re$; that is

$$P = E_{rms}^2 \Big/ \mathrm{Re}(\Re). \qquad (6)$$

Materials and methods

Figure 3 shows the complete experimental setup. A function generator (B&K 4011A) is connected to a power amplifier (ENI 3100L), which actuates the transducer. Based on some of our earlier work, which explores the level of thrust with a range of voltages and frequencies, the source function is chosen to be a sinusoid with varying voltages. The ENI unit amplifies at a gain of 50dB for a 50Ω load impedance. Voltage to the amplifier is increased incrementally in steps of $0.2V_{pp}$ up to a maximum of $1V_{pp}$, which corresponds to the output limit of the ENI unit. The output power to the transducer depends on the transducer load capacitance and electrical impedance, and is not explicitly controlled.

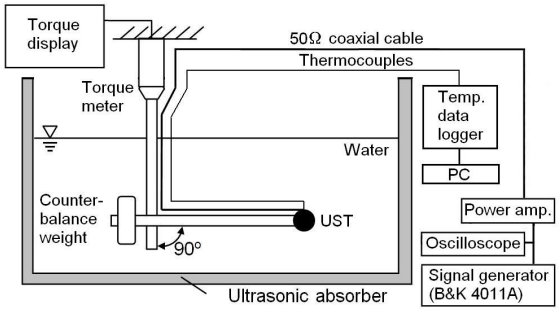

Figure 3. The experimental setup used to measure the UST temperature and thrust at the same time. Thrust is generated in the normal direction and out of the page.

The PZT measures 50mm in diameter and 2.1mm thick, resonating at around 1MHz. The epoxy cast layer is designed to be 0.6mm thick, with the same diameter as the transducer but the o-ring seals part of it, and only 42.2mm of the diameter is exposed to the water. The UST is vertically positioned with the surface facing the side wall of the 1.2×0.6×0.6m water tank, submerged at 0.2m from the bottom of the tank. Tap water is filled and stood for at least one day before the experiment begins, and ambient water temperature is regularly maintained at 21.5°C with sufficient cooling. Water is filled up to a depth of 0.45m.

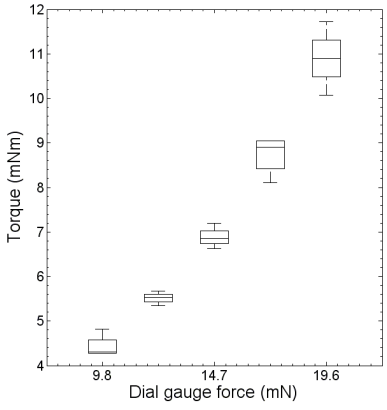

Figure 4. Calibration of the torque meter. Each of the five points shown is a distribution of four separate force applications using a sensitive dial gauge.

A precise torque meter measures the moment of the actuated UST thrust acting on an L-shaped arm. Given its known geometrical dimensions, the moment can be accurately and repeatably measured and converted into thrust as indicated in the calibration plot in Figure 4. From the manufacturer, the torque meter accuracy is ±0.09mN·m, and the effect of absolute error in the calibration thrust force averages about ±0.6mN, when a dial gauge presses on the UST, positioned 0.5m from the torque axis of the L-arm. Hence the total force uncertainty is about 0.8mN. Torque calibration is performed prior to all test sets.

The sensing tip of eight AWG 36 T-type (copper-constantan) thermocouples (SW-TTC2-F36-CL1) is attached to the transducer surface at five locations; T1 (north), T2 (east), T3 (west), T4 (south), and T5 (center) when viewed face-on as shown in Figure 5. Thermal grease is applied to the junction of the thermocouples for improved thermal contact and each junction is fixed to the surface with a small adhesive tape. All thermocouples measure 2m in length and each terminates at a type-T miniature plug (CN001-T) is plugged into an Eight Channel Thermocouple Logger (OctTemp, MadgeTech), which has corrected cold-junction compensation internally for improved accuracy and response time. Each of the thermocouple is wrapped with an electromagnetic interference (EMI) tape and grounded to remove any RF amplifier interference. All temperature sensors have been calibrated by the manufacturer and are prescribed with an accuracy of ±0.5°C. Temperature data is sampled at 4Hz for all channels. The data logger has a background temperature noise of less than 0.1°C. Overall, temperature measurement uncertainty is estimated to be ±1°C in all cases. We consider a quasi-steady state of heat transfer to be defined by a temperature change of 0.2°C in a minute for 3 minutes.

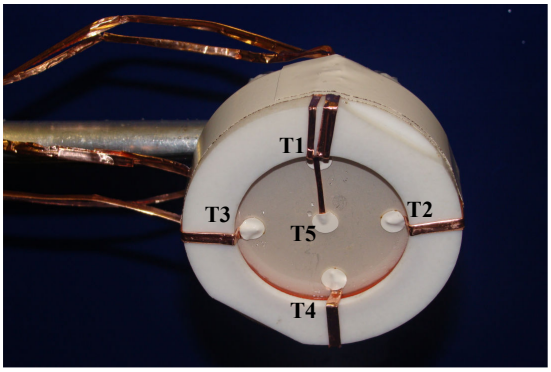

Figure 5. Locations of thermocouples attached to the surface of the UST; T1 (north), T2 (east), T3 (west), T4 (south), and T5 (center). Thermocouple cables are wrapped with RFI tape to ground RF interference.

The temperature versus time plot for locations T1 to T5 under increasing electrical power is shown from Figure 6 to 10. Each temperature profile at a particular applied power is repeated four times independently under ambient water conditions. The experiment begins by recording 5 seconds of ambient water temperature, after which the power amplifier is switched on for about 9mins. During this time, the transducer is observed to increase its temperature steadily and then maintain an approximately constant temperature. 9mins into the actuation, all thermocouple achieve a quasi-steady state and the power amplifier is switched off. Cooling proceeds for another 10mins and the tank is allowed to settle. Ambient temperature of the water tank is monitored separately at the start and end of the experiment, and further cooling is allowed if the ambient water temperature increased significantly.

Table 1 tabulates the steady-state temperature at all 5 locations on the transducer. Their respective standard deviation is also shown. Generally, increasing the input voltage ($0.2V_{pp}$ to $1.0V_{pp}$) to the amplifier increases the temperature recorded on the transducer surface. We note that T2 and T3 have a lower temperature compared to T1, T4, and T5. The core

wire of the coaxial is soldered at the air-backed side near the T4 position while the shielding is soldered near T3. We believe T4 could be a localized heating source although generally the PZT, which has two faces coated with silver compound, also increases in temperature. At thermal equilibrium, T1 displays a higher temperature even though it is furthest away from the coaxial core. We cannot explain why T1 experiences a higher temperature despite averaging four sets of repeated data. The mean surface temperature and output power from the amplifier are also recorded in the table.

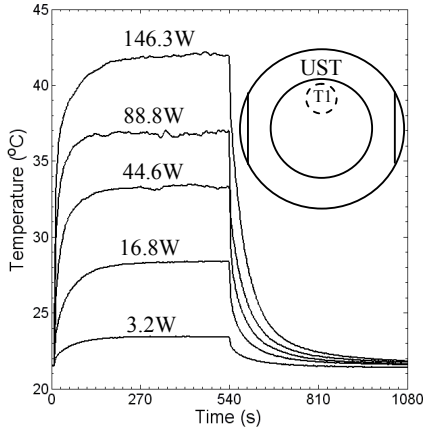

Figure 6. Temperature response at location T1 (north).

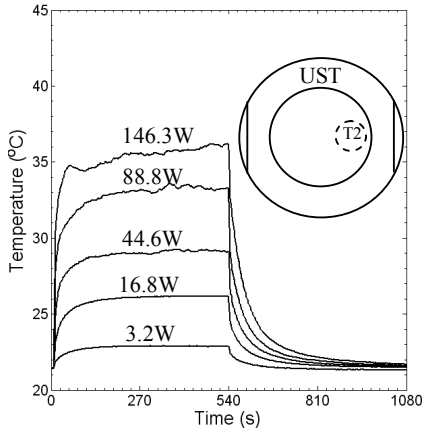

Figure 7. Temperature response at location T2 (east).

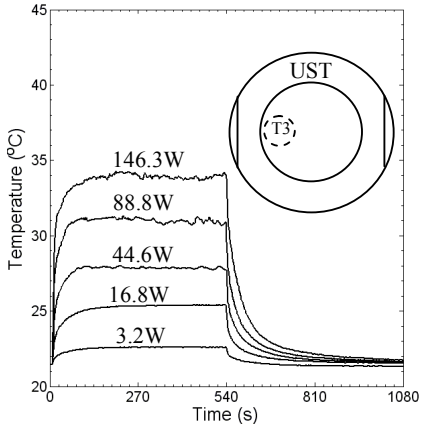

Figure 8. Temperature response at location T3 (west).

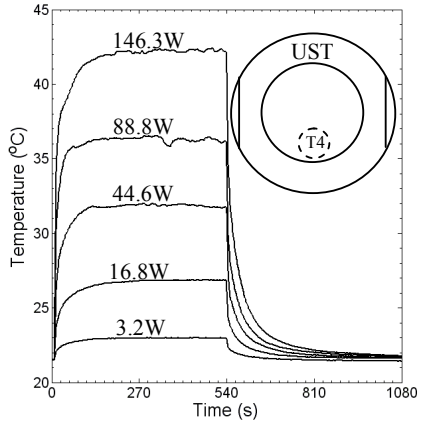

Figure 9. Temperature response at location T4 (south).

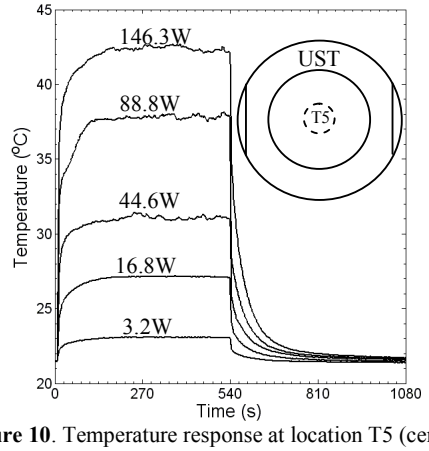

Figure 10. Temperature response at location T5 (center).

Table 1. Table of the input voltages to the amplifier and its corresponding UST steady-state surface temperatures. STD: standard deviation; Temp: temperature on the UST surface. The mean surface temperature and electrical power are also recorded.

	$0.2V_{pp}$		$0.4V_{pp}$		$0.6V_{pp}$		$0.8V_{pp}$		$1.0V_{pp}$	
	STD	T_e (°C)	STD	T_e (°C)	STD	T_e (°C)	STD	T_e (°C)	STD	T_e (°C)
T1	0.1	23.4	0.3	28.3	0.7	33.3	0.5	36.8	0.5	41.9
T2	0.1	22.8	0.2	26.1	0.5	29.1	0.2	33.2	0.3	35.7
T3	0.1	22.5	0.2	25.3	0.6	27.8	0.4	30.9	0.8	33.8
T4	0.03	22.9	0.3	26.8	0.3	31.8	0.3	36.2	1.0	42.2
T5	0.1	23.0	0.3	27.1	0.6	31.0	0.6	37.8	1.2	42.4
Mean temp (°C)		22.9		26.7		30.6		35.0		39.2
Electrical power (W)	3.2		16.8		44.6		88.8		146.3	

Table 2 summarizes the input voltage, output voltage, output power of the amplifier, and the corresponding thrust. Four sets of repeated input voltages are tabulated to demonstrate the consistency of the thrust generated.

Table 2. Table of output power from the amplifier and the corresponding thrust generated. Four sets of repeated input voltage data are shown. Ambient tank temperature is maintained at 21.5°C.

Input voltage (V_{pp})	Output voltage (V_{rms})	Output power (W)	Thrust (mN)
0.2	13	3.2	4.59
0.4	30	18.0	7.08
0.6	48	45.6	10.85
0.8	67	90.4	14.85
1.0	86	147.8	16.43
0.2	13	3.2	4.44
0.4	29	16.8	7.01
0.6	47	43.6	10.70
0.8	66	87.2	14.77
1.0	84	141.8	16.50
0.2	12	3.2	4.59
0.4	28	15.6	6.93
0.6	47	43.6	10.70
0.8	66	87.2	14.62
1.0	86	147.8	16.35
0.2	13	3.2	4.52
0.4	29	16.8	6.86
0.6	48	45.6	10.78
0.8	67	90.4	14.85
1.0	86	147.8	16.50

Using the two extreme right columns of Table 2, a plot of power versus thrust is shown in Figure 11. From Equation (6), the acoustic efficiency of the UST can be worked out, which essentially is the gradient at each cluster of points multiply by the speed of sound in the water, c. Generally at lower power, the efficiency is higher, however, effective thrust is also lower. As the power increases, efficiency declines rapidly and Figure 11 illustrates the trend. In Figure 11, it can be seen that generated thrust starts to decline at higher output power. From Equation (5) and (6), the thrust generated predicts a linear relationship expressed by $Thrust = \frac{\eta P}{c}$. However, as we discuss below, the acoustic efficiency and electrical impedance is observed to vary approximately in a first-order fashion as E_{rms} increases. Ultrasonic thrust appears to begin to saturate near 16mN.

THERMAL LOSSES OBSERVED

To calculate the averaged convective heat transfer, we use the lumped-capacity solution for a heated body transferring heat into the water by free convection. The solution can be solved with $T(t = 0)$ to give [11]

$$T = \left(T_e - T_\infty\right)e^{-t/\tau} + T_\infty \qquad (7)$$

where T (°C) is the time-variant temperature of the epoxy with respect to time t (s), T_e (°C) is the averaged temperature of the epoxy surface at T5 – from Table 1, and T_∞ (°C) is the ambient tank temperature. $\tau = \frac{\rho_e c_e V_e}{\bar{h} A_e}$ is the time constant of the cooling process, where ρ = 1200 kg/m^3 is the density of the epoxy, c_e = 1110 J/kg·°C is the specific heat capacity of epoxy, $V_e = 8.4\times10^{-7}$m^3 is the volume of the epoxy through which sound transmits, $\bar{h}$ (W/m^2·°C) is the average convective heat transfer coefficient, and A_e (m^2) is the cross-sectional area of the epoxy through which sound transmits. The location of the thermocouple on the epoxy layer is chosen at T5 because the linearized convective film would be mostly established.

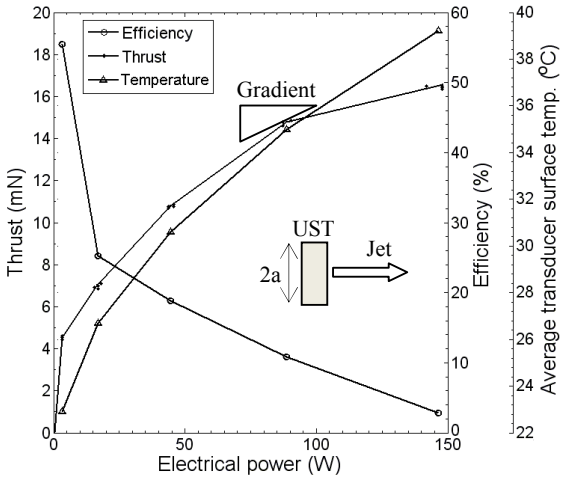

Figure 11. Thrust force generated, acoustic efficiency, and average surface temperature versus the electrical power driving the UST. Gradients of tangent at each of the clusters of thrust points indicate the UST efficiency. Low power operation generally gives higher efficiency, but at the expense of a lower thrust driving the UST. At higher output power, thrust generally begins to saturate.

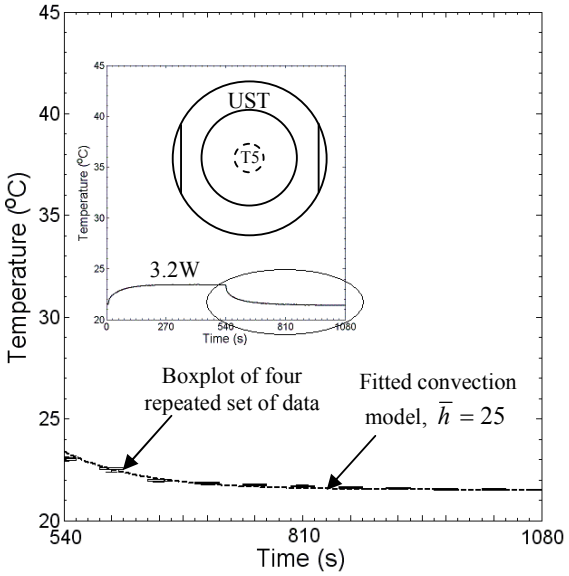

Figure 12. An example of heat loss profile of the UST at 3.2W output power. An increase in heat transfer rate is associated with an increase in surface temperature.

As an example, at 3.2W, we represent the four repeated sets of T5 temperatures from Table 2 in a boxplot for time t > 540secs as shown in Figure 12. Using Equation (7), we are able to plot a line through the data using least mean square fitting for a best value in $\bar{h}$. The convective coefficient will vary as the transducer surface temperature increases and this was found to be $\bar{h}$ = [25, 24, 22, 18, 14]W/m^2.°C as input power increases from 3.2 to 146.3W. Next, we use the $\bar{h}$ values and the mean transducer surface temperature tabulated in Table 1 to calculate the convective heat transfer rate into the water using Equation (3) to give Q_c = [0.052, 0.177, 0.281, 0.340, 0.347]W.

Most of this transmitted heat energy is convected away into the water as the surface of the transducer heats up. With this knowledge and the acoustic efficiency plot in Figure 11, where efficiency decline rapidly as output power increases, we can see that the supplied electrical power has been significantly converted into heat energy while thrust increased diminutively – that net thrust begins to saturate between 88.8W to 146.3W. In the region of the saturated thrust, we also note an increase in heating of the transducer as the power applied is increased further, explaining the fundamental cause of loss of converted electrical power.

The superfluous heat, Q_l (W), can be calculated using

$$Q_l = \frac{(T_{mid} - T_e)}{R_{eq}} \tag{8}$$

where the equivalent thermal resistance, $R_{eq} = \frac{x_p\left(1/\pi^2 + 1/4\right)}{4 k_p A_p} + \frac{x_e}{k_e A_e}$, for the transducer distance from $x = 0$ to the epoxy surface. We plot this heat loss against the amplifier output voltage, E_{rms}, in Figure 13. Introducing a dimensionless parameter, Q_l/P, which is the ratio of the heat loss energy (Equation (8)) to the electrical power supplied (Equation (6)), as

$$\frac{Q_l}{P} = \frac{(T_{mid} - T_e)\mathrm{Re}(\Re)}{R_{eq} E_{rms}^2}. \tag{9}$$

We refer to this parameter as the lossy ratio. A large lossy ratio means more electrical energy has been converted to superfluous heat and vice versa. This ratio is also plotted in Figure 13. Note that although the minimum of the graph signifies minimal heat loss to the electrical power supplied, it does not indicate the maximum thrust.

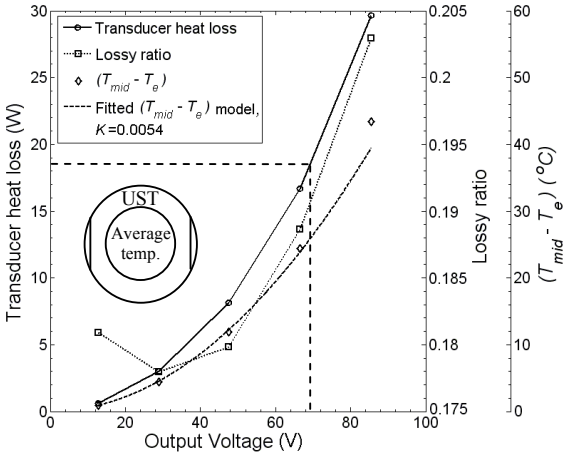

Figure 13. Superfluous heat loss through the surface of the UST versus output voltage, E_{rms}. An increase in output voltage is generally associated with an increase in heat loss. The minimum of the lossy curve signifies the least heat loss in the system. Higher heat loss ratio means more electrical energy is converted to heat losses instead of thrust.

To determine the maximum useable thrust without significant loss due to heating, we will consider acoustic efficiency above 10% to be worthy of pursuing. From Figure 11, the electrical power necessary to generate 10% efficiency should be less than 95W. Using Equation (6), where $\Re = 50\Omega$, E_{rms} is calculated to be 69V. When this voltage is applied across the transducer, from Figure 11, a UST thrust of about 15mN can be expected. Obviously increasing the voltage will increase the thrust but not appreciably; instead most added energy will be converted as heat losses.

Finally, we verify from Equation (1) that T_{mid} is not higher than the Curie temperature of the transducer, specified by the manufacturer to be at 320°C. Equation (4) is substituted into (3) to determine T_p, which is then substituted into Equation (1) together with (2). C = [11.26, 11.38, 11.81, 12.53, 13.62]nF and tan $\delta \approx 0.4\%$. The calculated values are T_{mid} = [23.84, 31.12, 42.49, 59.35, 82.59]°C with averaged output voltage as E_{rms} = [12.75, 29, 47.5, 66.5, 85.5]V. We also plot $T_{mid} - T_e$ versus E_{rms} in Figure 13 and show that it corresponds proportionally in a quadratic form, that is $T_{mid} - T_e \propto E_{rms}^2$, which equals to $T_{mid} - T_e = KE_{rms}^2$, with K as the constant of proportionality. Therefore, Equation (9) is also equivalent to

$$\frac{Q_l}{P} = \frac{K\,\mathrm{Re}(\Re)}{R_{eq}}. \tag{10}$$

We also validate that the Biot number, $Bi \ll 1$, which suggests that temperature within the transducer is relatively even. From the above parameters, $Bi = \bar{h}x_e/k_e$ = [0.0682, 0.0655, 0.0600, 0.0491, 0.0382]. This condition must also be satisfied for lump-capacity solution to be accurate.

CONCLUSIONS

We have studied the heating of ultrasonic transducers under conditions of thrust production. In view of practical application of the ultrasonic transducer in the medical field, it has been reported that clinical ultrasonic probes generate considerable heat when driven at off-resonance frequencies [6]. Most medical ultrasonic devices have a safety regulation on the level of power that the transducer can produce; for example, the IEC Standard 60606-2-37 limits the surface temperature of ultrasonic transducer to 43°C. In extreme cases, ultrasonic probes could reach a steady-state temperature of 80°C in ambient air at 25°C; obviously this is not suitable for human contact in practise. While the UST is not subject to complying with this standard, a UST device is still limited by heat losses in terms of damage, and because high temperature conditions still suffer a saturation of thrust.

It may be possible to minimize or harness heat for recycling in the UST system architecture, or even recoup it through specialized nozzle appendages so as to enhance efficiency. For example, the backing layer of the transducer can be ventilated or cooled to remove heat. Deardorff *et al.* [12, 13] demonstrated using a water-cooling system and reported not only it does not reduce the acoustic intensity or beam distribution, but also allows more than 45W additional power supplied to the transducer. Indeed, its thrust assistive quality remains to be investigated.

REFERENCES

[1] W. Trimmer and R. Jebens, "Actuators for micro robots," in *Proceedings. 1989 IEEE International Conference on Robotics and Automation (Cat. No.89CH2750-8), 14-19 May 1989*, Washington, DC, USA, 1989, pp. 1547-52.

[2] Y.-L. Cheng and J.-H. Lai, "Fabrication of meso-scale underwater vehicle components by rapid prototyping process," *Journal of Materials*

Processing Technology, vol. 201, pp. 640-644, 2008.

[3] A. C. H. Tan and F. S. Hover, "Correlating the ultrasonic thrust force with acoustic streaming velocity," presented at the Proceedings of the International Ultrasonics Symposium Rome, Italy, 2009.

[4] C. B. Panchal*, et al.*, "Biofouling control using ultrasonic and ultraviolet treatments," Department of Energy, Office of Scientific and Technical Information (DOE-OSTI)December 31 1995.

[5] S.-W. Zhou and C. A. Rogers, "Heat generation, temperature, and thermal stress of structurally integrated piezo-actuators," *Journal of Intelligent Material Systems and Structures,* vol. 6, pp. 372-379, 1995.

[6] F. A. Duck*, et al.*, "Surface heating of diagnostic ultrasound transducers," *British Journal of Radiology,* vol. 62, pp. 1005-13, 1989.

[7] W.-S. Ohm*, et al.*, "Prediction of surface temperature rise of ultrasonic diagnostic array transducers," *IEEE Transactions on Ultrasonics, Ferroelectrics, and Frequency Control,* vol. 55, pp. 125-135, 2008.

[8] S. Sherrit*, et al.*, "Characterization of transducers and resonators under high drive levels," in *2001 IEEE Ultrasonics Symposium. Proceedings. An International Symposium, 7-10 Oct. 2001*, Piscataway, NJ, USA, 2001, pp. 1097-100.

[9] A. C. H. Tan and F. S. Hover, "Ultrasonic propulsion in small underwater vehicles," *IEEE Journal of Oceanic Engineering,* to appear 2010.

[10] E. M. Allison*, et al.*, "Ultrasonic propulsion," *Journal of Propulsion and Power,* vol. 24, pp. 547-553, 2008.

[11] J. H. Lienhard IV and J. H. Lienhard V, *A heat transfer textbook* Cambridge, Mass. : Phlogiston Press, 2002.

[12] D. L. Deardorff and C. J. Diederich, "Angular directivity of thermal coagulation using air-cooled direct- coupled interstitial ultrasound applicators," *Ultrasound in Medicine and Biology,* vol. 25, pp. 609-622, 1999.

[13] D. L. Deardorff and C. J. Diederich, "Ultrasound applicators with internal water-cooling for high-powered interstitial thermal therapy," *IEEE Transactions on Biomedical Engineering,* vol. 47, pp. 1356-1365, 2000.